

Topological Hall effect in bulk ferromagnet Cr_2Te_3 embedded with black-phosphorus-like bismuth nanosheets

Liang Zhou,^{1,*} Junshu Chen,^{1,*} Xiaobin Chen,^{2,1,*} Bin Xi,³ Yang Qiu,⁴ Junwei Zhang,⁵ Linjing Wang,¹ Runnan Zhang,¹ Bicong Ye,¹ Pingbo Chen,¹ Xixiang Zhang,⁵ Guoping Guo,⁶ Dapeng Yu,¹ Jia-Wei Mei,^{1,†} Fei Ye,^{1,‡} Gan Wang,^{1,7,§} and Hongtao He^{1,¶}

¹*Institute for Quantum Science and Engineering, and Department of Physics, Southern University of Science and Technology, Shenzhen 518055, China*

²*School of Science, Harbin Institute of Technology, Shenzhen 518055, China*

³*College of Physics Science and Technology, Yangzhou University, Yangzhou 225002, China*

⁴*Materials Characterization and Preparation Center, Southern University of Science and Technology, Shenzhen 518055, China*

⁵*King Abdullah University of Science and Technology (KAUST), Physical Science and Engineering, Thuwal 23955-6900, Saudi Arabia*

⁶*Key Laboratory of Quantum Information, CAS, University of Science and Technology of China, Hefei 230026, China*

⁷*Shenzhen Key Laboratory of Quantum Science and Engineering, Shenzhen 518055, China.*

(Dated: March 18, 2019)

We implement the molecular beam epitaxy method to embed the black-phosphorus-like bismuth nanosheets into the bulk ferromagnet Cr_2Te_3 . As a typical surfactant, bismuth lowers the surface tensions and mediates the layer-by-layer growth of Cr_2Te_3 . Meanwhile, the bismuth atoms precipitate into black-phosphorus-like nanosheets with the lateral size of several tens of nanometers. In Cr_2Te_3 embedded with Bi-nanosheets, we observe simultaneously a large topological Hall effect together with the magnetic susceptibility plateau and magnetoresistivity anomaly. As a control experiment, none of these signals is observed in the pristine Cr_2Te_3 samples. Therefore, the Bi-nanosheets serve as seeds of topological Hall effect induced by non-coplanar magnetic textures planted into Cr_2Te_3 . Our experiments demonstrate a new method to generate a large topological Hall effect by planting strong spin-orbit couplings into the traditional ferromagnet, which may have potential applications in spintronics.

Introduction – When it flows in the presence of a static magnetic field in the perpendicular direction, the electron is deflected by the Lorentz force and gives rise to the Hall effects identified by a transverse resistivity [1]. The external magnetic field is not mandatory, however, ‘Berry curvature’ is essential to produce a Hall effect [2]. The spin-orbit coupling in the magnetic system generates the anomalous Hall effect (AHE) associated with the Berry curvature in momentum space [2]. The non-coplanar magnetic texture could have a chiral real space configuration of the local moments, which have unique geometrical or topological properties in real space leading to the topological Hall effect (THE) [3–15]. THE is usually observed in mainly three families of materials, such as the chiral magnetic B20 compounds (MnSi, FeGe, $\text{Fe}_{1-x}\text{Co}_x\text{Si}$, etc.) with broken inversion symmetry [8, 16–20], the metallic ferromagnet/paramagnet bilayers with artificial Dzyaloshinsky-Moriya (DM) interactions at the interface [9–11, 21], and magnetically doped topological insulators [12, 22]. The THE is a signature of the chiral magnetic texture, *i.e.* magnetic skyrmions [5, 23–25], which may have potential applications in spintronics.

THE originates in the entanglement of ferromagnets and strong spin-orbit couplings. To expand the family of ‘THE materials’, it is of significant interests to efficiently insert strong spin-orbit couplings into traditional ferro-

magnets, which is still challenging so far. Among many typical ferromagnets, the study of chromium tellurides has a long history and can be traced back to 1935 [26]. Depending on the stoichiometric ratio, Cr_{1-x}Te has a rich structural phase diagram with Curie temperatures ranging from 170 K to 340 K [26]. Very recently, the Cr_2Te_3 thin film with a high-quality single crystalline structure has been synthesized using the molecular beam epitaxy (MBE) technique, which shows a strong perpendicular magnetic anisotropy and a large magnetic moment per Cr atom about $2.8 \mu_B$ [27, 28]. If strong spin-orbit coupling elements can be doped in an appropriate way, Cr_2Te_3 would exhibit significant THE with the onset temperature close to the Curie temperature. A convenient candidate is bismuth, which is well known not only for its strong spin-orbit coupling, but also as a typical surfactant to achieve the layer-by-layer growth mode in MBE [29, 30]. Furthermore, bismuth has various atom-thick layer structures, such as bismuthene [31] and the very unusual puckered-layer structure [32, 33] similar to black phosphorus [34].

In this Letter, we report a new efficient route towards producing “THE materials” by embedding black-phosphorus-like bismuth nanosheets into the bulk ferromagnet Cr_2Te_3 . We reveal a large, high-temperature topological Hall effect together with magnetic susceptibility plateau and magnetoresistivity anomaly. As a con-

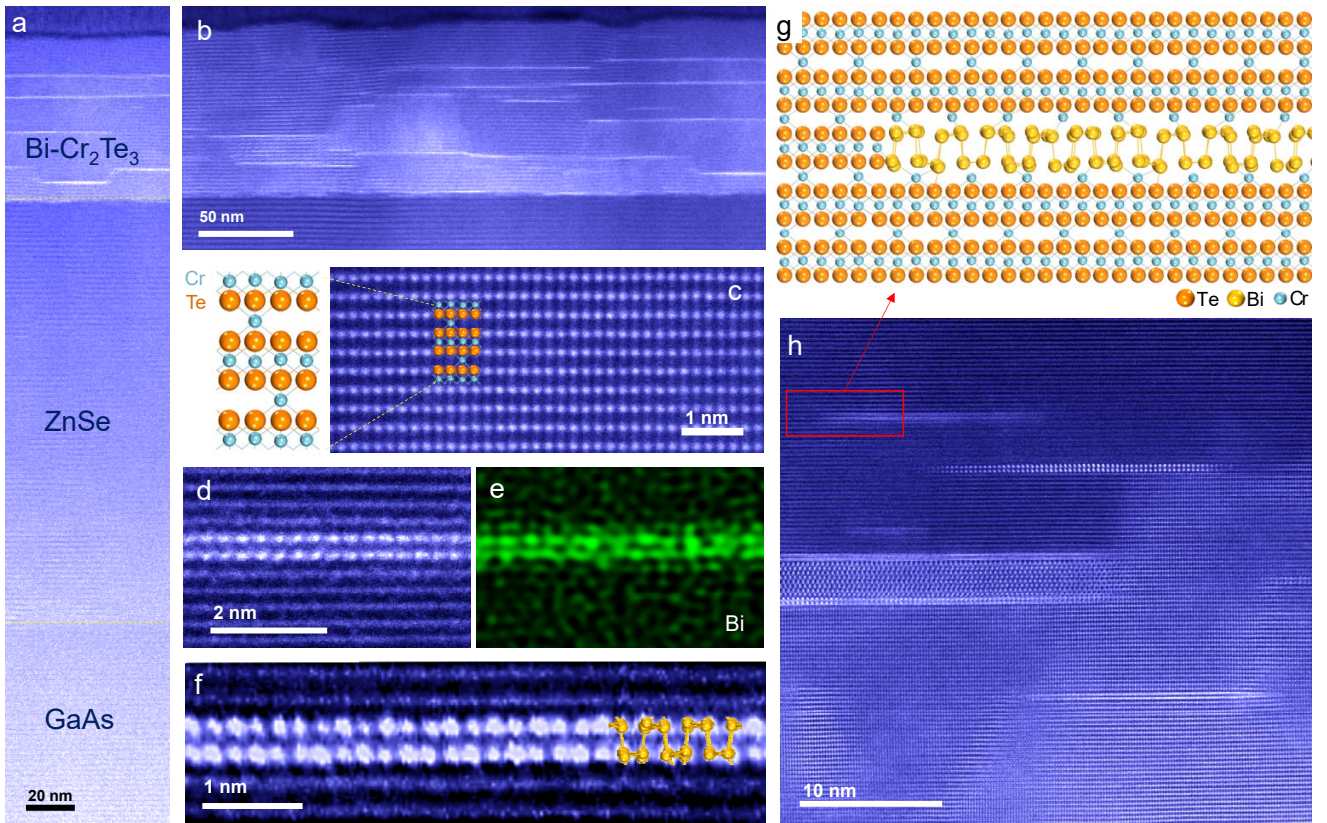


FIG. 1. HAADF STEM images of the MBE-grown Bi-embedded Cr_2Te_3 . (a) Cross-sectional HAADF STEM image of a sliced MBE-grown Cr_2Te_3 sample. The visible white filaments inside the Cr_2Te_3 layer are bismuth nanosheets. (b) Landscape STEM image of a Cr_2Te_3 sample. (c) High resolution STEM image of crystalline Cr_2Te_3 . Note that the Cr atoms are invisible in the STEM image. (d) and (e) STEM image and EDS mappings for the distribution of Bi element. (f) STEM image with enlarged scale showing a bilayer bismuth sandwiched between layers of Cr_2Te_3 . (g) Atomic configuration (side view) of a bismuth nanosheet embedded Cr_2Te_3 structure. (h) High resolution STEM image for several Bi nanosheets embedded in the Cr_2Te_3 layer.

trol experiment, none of these signals is observed in the pristine Cr_2Te_3 samples, revealing the critical role of Bi-nanosheets with strong spin-orbit coupling. Therefore, the Bi-nanosheets serve as seeds of spin-orbit couplings planted into Cr_2Te_3 to generate THE. We also discuss the magnetic skyrmion scenario accounting for our experimental results.

Sample growth and characterizations – The growth of Bi-intercalated Cr_2Te_3 thin films were performed on semi-insulating epi-ready GaAs(111)B substrates in a home-built molecular beam epitaxy system with a base vacuum of MBE better than 5×10^{-10} torr. Prior to the growth of Cr_2Te_3 , the GaAs(111)B substrate was first deoxidized at 580°C until streaky RHEED patterns appeared, followed by a deposition of 150 nm ZnSe buffer layer for smoothing the voids of GaAs induced by the deoxidation. Cr_2Te_3 thin film were grown by co-evaporating Bi (99.995%), Cr (99.999%), and Te (99.999%) from Knudsen cells with a flux ratio of 2:1:10 at $T_{\text{substrate}} = 260^\circ\text{C}$. A spherical aberration corrected

scanning transmission electron microscopy (STEM) were employed for performing systematic structure and chemical analyses.

The Cr_2Te_3 thin films were grown on the GaAs(111) substrate with a buffer layer of ZnSe, as shown in the cross-sectional high angle annular dark field (HAADF) STEM image in Fig. 1 (a). During the growing process a concurrent bismuth flux was applied together with Cr and Te fluxes. The participation of bismuth atoms can lower the surface tensions resulting in a surfactant-mediated layer-by-layer growth mode instead of a three-dimensional cluster mode [29, 30]. In fact, we observed the extended streaky reflection high-energy electron diffraction (RHEED) patterns during the entire growing process. The X-ray diffraction measurement also shows that Bi-embedded samples have much better crystalline quality than non-Bi-embedded ones [35].

Figure. 1 (b) shows the landscape STEM image of a Cr_2Te_3 thin film embedded with Bi nanosheets, where a single crystalline structure is found with a sharp in-

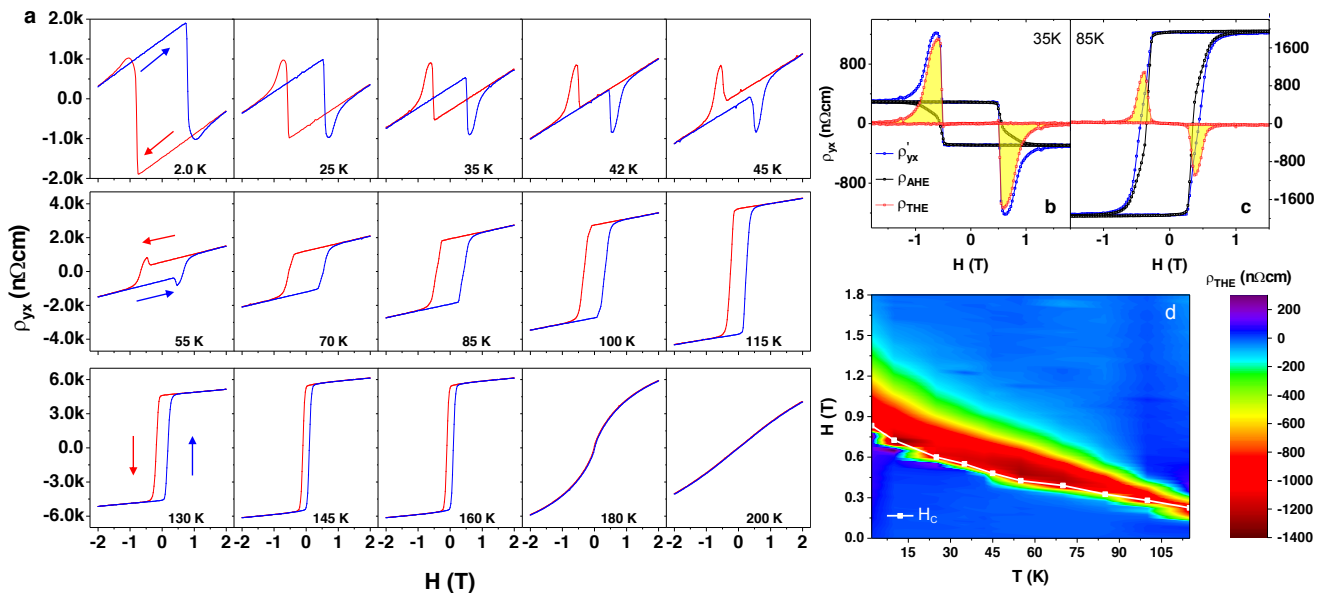


FIG. 2. Topological Hall Effect. (a) Magnetic field (H) dependence of Hall resistivity (ρ_{yx}) at various temperatures. The red (blue) curves were measured in decreasing (increasing) the magnetic field. (b) and (c) Extraction of THE contribution to Hall resistivity at 35 and 85 K. The topological Hall resistivity (ρ_{THE}) is obtained by subtracting the anomalous Hall resistivity (ρ_{AHE}) from ρ'_{yx} , where $\rho'_{yx} = \rho_{yx} - \rho_{\text{OHE}}$ and ρ_{OHE} is the ordinary Hall resistivity. (d) Color map of THE in the T - H plane. The temperature dependence of H_c which is determined by the magnetic hysteresis measurement is also plotted.

interface near the ZnSe buffer layer. The high-resolution STEM image of Cr_2Te_3 lattice in Fig. 1 (c) shows a typical NiAs-type lattice structure of the pristine Cr_2Te_3 oriented along [001] direction. The lattice constants of Cr_2Te_3 are determined to be $a = b = 6.81 \text{ \AA}$ and $c = 12.28 \text{ \AA}$. The atom distributions of a Bi nanosheet are revealed in Fig. 1 (d) and (e) by the atomically resolved energy dispersive X-ray spectroscopy (EDS) mapping, showing that the Bi atoms occupy Te sites to form a bilayer structure embedded in the Cr_2Te_3 lattice. The bismuth atoms precipitate into nanosheets with lateral size of several tens of nanometers, corresponding to the luminescent line segments in Fig. 1 (a) and (b). The atomically resolved STEM image given in Fig. 1 (f) further reveals that the bismuth nanosheet owns a bilayer structure with lattice constants $a = 4.5 \text{ \AA}$ and $c = 6.5 \text{ \AA}$, in a striking analogy to the puckered-layer structure of black phosphorus [34]. Fig. 1 (g) is the atomic configuration of a Bi-nanosheet embedding in the Cr_2Te_3 as shown in the high resolution STEM image in Fig. 1 (h). The embedded bilayer bismuth exhibits a slight distortion due to the interaction with Cr_2Te_3 .

Topological Hall effect – Then Bi-embedded Cr_2Te_3 samples hybridize strong spin-orbit couplings and ferromagnetism, and we observe a significant THE in the magneto-transport experiments. Fig. 2 is the THE result in a 60-nm-thick sample of Cr_2Te_3 embedded with Bi nanosheets. The Curie temperature (T_c) of the sample is determined to be 180 K from the temperature dependence of resistivity and magnetization [35]. Fig. 2 (a)

shows the double-sweep measurements of the Hall resistivity $\rho_{yx}(H)$ at various temperatures with the magnetic field H along the [001] direction. Above T_c , the Hall resistivity is linearly dependent on H , namely, $\rho_{\text{OHE}} = R_o H$ as expected for the ordinary Hall effect (OHE). Since the ordinary Hall coefficient $R_o > 0$ as shown in Fig. 2 (a), the charge carrier is of p -type and the density can also be estimated to be around 10^{21} cm^{-3} [35], coming from the unoccupied Cr-3d orbitals. Below T_c , a clear hysteresis behavior is observed, indicative of the anomalous Hall effect (AHE). The anomalous Hall resistivity depends on the magnetization M and is generally written as $\rho_{\text{AHE}} = R_a M$. There are usually three independent origins of the AHE, including the skew-scattering, side-jump and the Berry curvature in momentum space [2], which may have opposite contributions, thus possibly cancel with one another leading to a vanishing anomalous Hall coefficient R_a [28]. Indeed, we find the sign of R_a is reversed at $T \sim 42 \text{ K}$ with decreasing temperature, and no anomalous Hall resistivity is detected right at this temperature.

The most striking feature of the Hall resistivity curves is the emergence of abnormal peaks in the vicinity of the coercive field (H_c), as shown in Fig. 2 (a). These peaks show up regardless of the sign of R_a , even at $T = 42 \text{ K}$ where the AHE vanishes completely, indicating that these abnormal Hall resistivity peaks should have a different origin from the AHE. In fact these pronounced peaks can be attributed to the THE, which is related to the spin chirality of magnetic skyrmions [3–7]. Similar THE signal

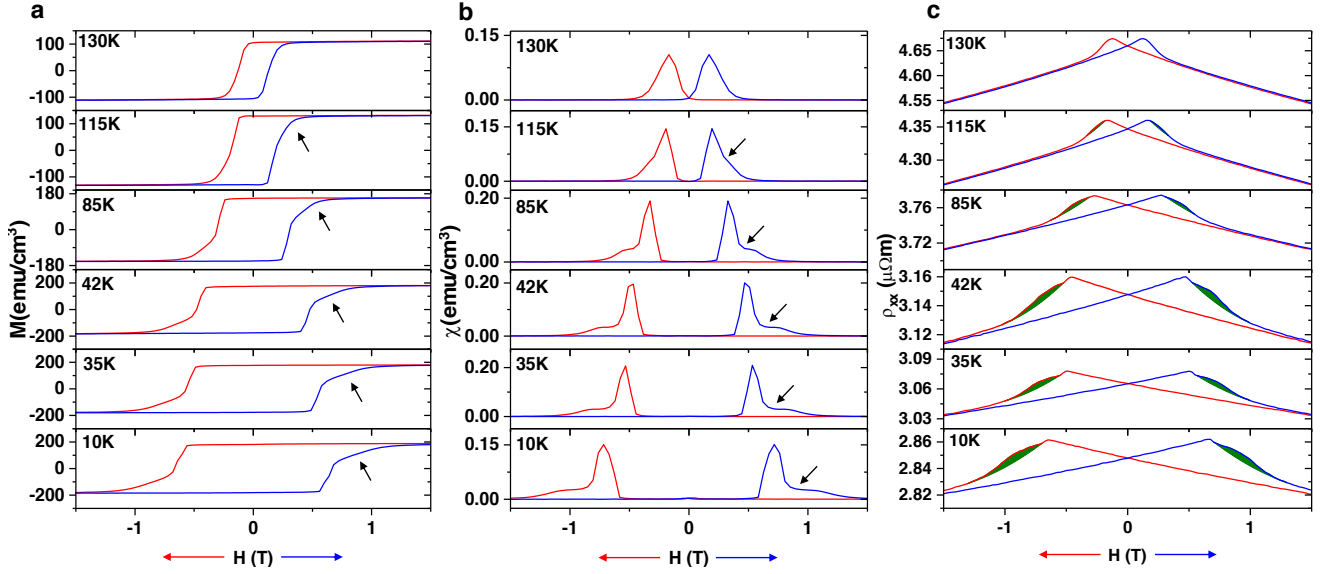


FIG. 3. Magnetization tail, magnetic susceptibility plateau, and magnetoresistivity anomaly. (a) and (b) Magnetic field dependence of magnetization and the corresponding susceptibility, respectively, at various temperatures. The magnetic susceptibility also displays a plateau as indicated by an arrow. (c) Magnetic field dependence of the longitudinal magnetoresistivity at various temperatures. A hump feature is clearly observed, in close correlation with the occurrence of THE.

was also observed in 45-nm-thick Bi-embedded Cr_2Te_3 samples [35]. The topological Hall resistivity can be extracted from the total Hall resistivity ρ_{yx} in the form $\rho_{\text{THE}} = \rho_{yx} - R_o H - R_a M$ [35]. Fig. 2 (b) shows the H -dependence of ρ_{AHE} and ρ_{THE} at $T = 35$ K, where we also plot $\rho'_{yx} \equiv \rho_{yx} - R_o H (= \rho_{\text{THE}} + \rho_{\text{AHE}})$ for comparison. Obviously, $\rho_{\text{AHE}}(H)$ and $\rho'_{yx}(H)$ almost coincide with each other, except in the region near the coercive field where the THE appears. The resultant ρ_{THE} and ρ_{AHE} at 85 K are plotted in Fig. 2 (c). Fig. 2 (d) is a phase diagram illustrating the strength of THE signals. Obviously, the THE occurs only in the vicinity of the coercive field, implying that the appearance of the non-zero spin chirality is associated with the magnetization reversal. It is worth noting that the maximum ρ_{THE} in our sample of Bi-embedded Cr_2Te_3 is around 1300 n Ω -cm, which is larger than that of $\text{SrRuO}_3/\text{SrIrO}_3$ [9] and one order of magnitude larger than that of the B20 chiral magnet (*e.g.*, MnSi) [8].

Magnetic susceptibility plateau and magnetoresistivity anomaly – Fig. 3 shows the temperature dependence of magnetization M , magnetic susceptibility $\chi(H) = \partial M(H)/\partial H$, and magnetoresistivity ρ_{xx} , respectively. Right in the region near the coercive field, the $M(H)$ curve shows an abnormal magnetization tail, which corresponds to a striking susceptibility plateau in the $\chi(H)$ curve, as indicated by arrows in Fig. 3 (a) and (b). Furthermore, as evident in Fig. 3 (c), the $\rho_{xx}(H)$ curve also exhibits a hump feature near H_c , indicative of a new scattering source for electronic transport. All these abnormal behaviors persist up to 115 K, similar to the THE shown in Fig. 2 (c). In the field region where THE appears, the

$M(H)$ curve exhibits a tail, indicating the emergence of nontrivial spin texture. The coincidence of the active regions of THE, magnetization tail, susceptibility plateau, and magnetoresistivity hump strongly suggests the same physical origin of them.

Discussions and conclusions – As a well established theory [3–7], the magnetic skyrmion can induce the THE owing to its nonvanishing spin chirality. Skyrmions can be identified directly by mapping the spin textures using small angle neutron scattering [16], Lorentz transmission electron microscopy [36], spin-resolved scanning tunneling microscopy [37], resonant x-ray scattering [38], or even magneto-optics [39]. However, the direct mapping of skyrmions is beyond the scope of this work, and is left to future investigations. We have checked our experimental results very carefully, and found that all our experimental details can be explained in terms of magnetic skyrmion scenario. Furthermore, the skyrmion is also supported in the numerical simulations with the input parameters derived from the first-principles of our system [40].

In Cr_2Te_3 with Bi nanosheet embedded, the magnetization saturates with all the local moments fully polarized in the high fields $H > H_c$, hence the scalar spin chirality $\vec{S}_i \cdot (\vec{S}_j \times \vec{S}_k)$ is zero and no THE occurs. Once the field reverses and exceeds the coercive field H_c , the moments in the bulk Cr_2Te_3 are flipped first, and those near the Bi-nanosheets are not completely flipped yet, but only twisted by the DM interactions (resulting from the hybridization between Bi and Cr orbitals), leading to the formation of magnetic skyrmions in the vicinity of the coercive field. The nonzero spin chiralities of these

skyrmions in turn give rise to the THE. This scenario is consistent with the measurements of magnetization and longitudinal magnetoresistivity as shown momentarily. Skyrmions display the topological paramagnetism [40], *i.e.*, the susceptibility plateaux and magnetization tails, which is related to the topological stability of the magnetic skyrmions and due to the slowing down of the flipping speed of skyrmion moments near H_c [41]. Furthermore, the magnetic texture of skyrmions is also a new scattering source accounting for the magnetoresistivity hump near H_c in Fig. 3 (c) [41].

To the best of our knowledge, it is the first time in the literature to observe all these skyrmion-induced features, THE, topological paramagnetism and magnetoresistivity anomaly, simultaneously in the same system. Therefore, it is very likely that our system hosts the magnetic skyrmions in the THE region. Detailed information of the magnetic skyrmions in Bi-embedded Cr_2Te_3 can be also derived from our experimental data [35]. We estimate the skyrmion size is about 14 nm, comparable with the lateral sizes of Bi nanosheets which may vary from 10 nm to 100 nm (see Fig. 1 (b)). Therefore, by controlling the diameter of the Bi-nanosheets, a single skyrmion can be obtained and its size may be further reduced in smaller Bi-nanosheets.

In conclusion, we have grown the bulk ferromagnet Cr_2Te_3 with the black-phosphorous-like bismuth nanosheet embedded. It is an efficient experimental approach to insert strong spin-orbit couplings into the traditional ferromagnet. The nanosheet serves as a ‘seed’ for the strong spin-orbit coupling planted into the bulk ferromagnet, and generates the non-trivial magnetic texture, signaled by a large topological Hall effect, topological paramagnetism and magnetoresistivity anomaly. This method can be applied to other bulk ferromagnetic systems, largely expanding the family of topological-Hall-effect materials.

We thank Z.Z. Du and H.Z. Lu for helpful discussions. This work was supported by the National Natural Science Foundation of China (No. 11574129, 11774143, 61734008, 51404293 and 11374135, 11774300), the National Key Research and Development Program of China (No. 2016YFA0301703), the Natural Science Foundation of Guangdong Province (No. 2015A030313840, and 2017A030313033), the State Key Laboratory of Low-Dimensional Quantum Physics (No. KF201602), Technology and Innovation Commission of Shenzhen Municipality (No. JCYJ20160531190254691, JCYJ20160531190535310, KQJSCX20170727090712763, ZDSYS201703031659262, and JCYJ20170412152334605). J.W.M was partially supported by the program for Guangdong Introducing Innovative and Entrepreneurial Teams (No. 2017ZT07C062). J. Zhang and X. Zhang were supported by King Abdullah University of Science and Technology (KAUST), Office of Sponsored Research (OSR) under

Award No: CRF-2015-2549-CRG4.

* These three authors contribute to this work equally.

† meijw@sustech.edu.cn

‡ yef@sustech.edu.cn

§ wangg@sustech.edu.cn

¶ heht@sustech.edu.cn

- [1] EH Hall, “On a new action of the magnet on electric currents,” *American Journal of Mathematics* **2**, 287–292 (1879).
- [2] Naoto Nagaosa, Jairo Sinova, Shigeki Onoda, A. H. MacDonald, and N. P. Ong, “Anomalous Hall effect,” *Rev. Mod. Phys.* **82**, 1539 (2010).
- [3] N. Nagaosa, X. Z. Yu, and Y. Tokura, “Gauge fields in real and momentum spaces in magnets: monopoles and skyrmions,” *Philos. Trans. Royal Soc. A* **370**, 5806 (2012).
- [4] N. Nagaosa and Y. Tokura, “Emergent electromagnetism in solids,” *Phys. Scr.* **2012**, 014020 (2012).
- [5] N. Nagaosa and Y. Tokura, “Topological properties and dynamics of magnetic skyrmions,” *Nat. Nanotech.* **8**, 899 (2013).
- [6] Jinwu Ye, Yong Baek Kim, A. J. Millis, B. I. Shraiman, P. Majumdar, and Z. Tešanović, “Berry Phase Theory of the Anomalous Hall Effect: Application to Colossal Magnetoresistance Manganites,” *Phys. Rev. Lett.* **83**, 3737 (1999).
- [7] P. Bruno, V. K. Dugaev, and M. Taillefumier, “Topological Hall Effect and Berry Phase in Magnetic Nanostructures,” *Phys. Rev. Lett.* **93**, 096806 (2004).
- [8] A. Neubauer, C. Pfleiderer, B. Binz, A. Rosch, R. Ritz, P. G. Niklowitz, and P. Böni, “Topological Hall Effect in the *A* Phase of MnSi,” *Phys. Rev. Lett.* **102**, 186602 (2009).
- [9] Jobu Matsuno, Naoki Ogawa, Kenji Yasuda, Fumitaka Kagawa, Wataru Koshihase, Naoto Nagaosa, Yoshinori Tokura, and Masashi Kawasaki, “Interface-driven topological Hall effect in SrRuO₃-SrIrO₃ bilayer,” *Sci. Adv.* **2**, e1600304 (2016).
- [10] K. Yasuda, R. Wakatsuki, T. Morimoto, R. Yoshimi, A. Tsukazaki, K. S. Takahashi, M. Ezawa, M. Kawasaki, N. Nagaosa, and Y. Tokura, “Geometric Hall effects in Topological Insulator Heterostructures,” *Nat. Phys.* **12**, 555 (2016).
- [11] Dapeng Zhao, Liguang Zhang, Iftikhar Ahmed Malik, Menghan Liao, Wenqiang Cui, Xinqiang Cai, Cheng Zheng, Luxin Li, Xiaopeng Hu, Ding Zhang, Jinxing Zhang, Xi Chen, Wanjuan Jiang, and Qikun Xue, “Observation of unconventional anomalous Hall effect in epitaxial CrTe thin films,” *Nano Res.* **11**, 3116 (2018).
- [12] Chang Liu, Yunyi Zang, Wei Ruan, Yan Gong, Ke He, Xucun Ma, Qi-Kun Xue, and Yayu Wang, “Dimensional Crossover-Induced Topological Hall Effect in a Magnetic Topological Insulator,” *Phys. Rev. Lett.* **119**, 176809 (2017).
- [13] Minhyea Lee, W. Kang, Y. Onose, Y. Tokura, and N. P. Ong, “Unusual Hall Effect Anomaly in MnSi under Pressure,” *Phys. Rev. Lett.* **102**, 186601 (2009).
- [14] N. Kanazawa, Y. Onose, T. Arima, D. Okuyama, K. Ohoyama, S. Wakimoto, K. Kakurai, S. Ishiwata, and

- Y. Tokura, "Large Topological Hall Effect in a Short-Period Helimagnet MnGe," *Phys. Rev. Lett.* **106**, 156603 (2011).
- [15] S. X. Huang and C. L. Chien, "Extended Skyrmion Phase in Epitaxial FeGe(111) Thin Films," *Phys. Rev. Lett.* **108**, 267201 (2012).
- [16] S. Mühlbauer, B. Binz, F. Jonietz, C. Pfleiderer, A. Rosch, A. Neubauer, R. Georgii, and P. Böni, "Skyrmion Lattice in a Chiral Magnet," *Science* **323**, 915 (2009).
- [17] S. V. Grigoriev, D. Chernyshov, V. A. Dyadkin, V. Dmitriev, S. V. Maleyev, E. V. Moskvina, D. Menzel, J. Schoenes, and H. Eckerlebe, "Crystal Handedness and Spin Helix Chirality in $\text{Fe}_{1-x}\text{Co}_x\text{Si}$," *Phys. Rev. Lett.* **102**, 037204 (2009).
- [18] H. Wilhelm, M. Baenitz, M. Schmidt, U. K. Rößler, A. A. Leonov, and A. N. Bogdanov, "Precursor Phenomena at the Magnetic Ordering of the Cubic Helimagnet FeGe," *Phys. Rev. Lett.* **107**, 127203 (2011).
- [19] Y. Tokunaga, X.Z. Yu, J.S. White, Henrik M. Rønnow, D. Morikawa, Y. Taguchi, and Y. Tokura, "A new class of chiral materials hosting magnetic skyrmions beyond room temperature," *Nat. Commun.* **6**, 7638 (2015).
- [20] K. Karube, J. S. White, N. Reynolds, J. L. Gavilano, H. Oike, A. Kikkawa, F. Kagawa, Y. Tokunaga, Henrik M. Rønnow, Y. Tokura, and Y. Taguchi, "Robust metastable skyrmions and their triangular-square lattice structural transition in a high-temperature chiral magnet," *Nat. Mater.* **15**, 1237 (2016).
- [21] M. Bode, M. Heide, K. von Bergmann, P. Ferriani, S. Heinze, G. Bihlmayer, A. Kubetzka, O. Pietzsch, S. Blügel, and R. Wiesendanger, "Chiral magnetic order at surfaces driven by inversion asymmetry," *Nature* **447**, 190 (2007).
- [22] F. Ye, G. H. Ding, H. Zhai, and Z. B. Su, "Spin helix of magnetic impurities in two-dimensional helical metal," *EPL* **90**, 47001 (2010).
- [23] T.H.R. Skyrme, "A unified field theory of mesons and baryons," *Nucl. Phys.* **31**, 556 (1962).
- [24] A. N. Bogdanov and D. A. Yablonskii, "Thermodynamically stable "vortices" in magnetically ordered crystals. the mixed state of magnets," *Sov. Phys. JETP* **68**, 101 (1989).
- [25] A. Bogdanov and A. Hubert, "Thermodynamically stable magnetic vortex states in magnetic crystals," *J. Magn. Mater.* **138**, 255 (1994).
- [26] Haakon Haraldsen and Elisabeth Kowalski, "Magnetochemische Untersuchungen. XVII. Das magnetische Verhalten der Chalkogenide des zweiwertigen Chroms," *Z. Anorg. Allg. Chem.* **224**, 329–336 (1935).
- [27] Anupam Roy, Samaresh Guchhait, Rik Dey, Tanmoy Pramanik, Cheng-Chih Hsieh, Amritesh Rai, and Sanjay K Banerjee, "Perpendicular magnetic anisotropy and spin glass-like behavior in molecular beam epitaxy grown chromium telluride thin films," *ACS nano* **9**, 3772 (2015).
- [28] L. Zhou, J. S. Chen, Z. Z. Du, X. S. He, B. C. Ye, G. P. Guo, H. Z. Lu, G. Wang, and H. T. He, "Magnetotransport properties of $\text{Cr}_{1-\delta}\text{Te}$ thin films with strong perpendicular magnetic anisotropy," *AIP Adv.* **7**, 125116 (2017).
- [29] M. Copel, M. C. Reuter, Efthimios Kaxiras, and R. M. Tromp, "Surfactants in epitaxial growth," *Phys. Rev. Lett.* **63**, 632 (1989).
- [30] H. A. van der Vegt, H. M. van Pinxteren, M. Lohmeier, E. Vlieg, and J. M. C. Thornton, "Surfactant-induced layer-by-layer growth of Ag on Ag(111)," *Phys. Rev. Lett.* **68**, 3335 (1992).
- [31] F. Reis, G. Li, L. Dudy, M. Bauernfeind, S. Glass, W. Hanke, R. Thomale, J. Schäfer, and R. Claessen, "Bismuthene on a SiC substrate: A candidate for a high-temperature quantum spin Hall material," *Science* **357**, 287 (2017).
- [32] T. Nagao, J. T. Sadowski, M. Saito, S. Yaginuma, Y. Fujikawa, T. Kogure, T. Ohno, Y. Hasegawa, S. Hasegawa, and T. Sakurai, "Nanofilm Allotrope and Phase Transformation of Ultrathin Bi Film on Si(111)- 7×7 ," *Phys. Rev. Lett.* **93**, 105501 (2004).
- [33] Shin Yaginuma, Katsumi Nagaoka, Tadaaki Nagao, Gustav Bihlmayer, Yury M. Koroteev, Eugene V. Chulkov, and Tomonobu Nakayama, "Electronic Structure of Ultrathin Bismuth Films with A7 and Black-Phosphorus-like Structures," *J. Phys. Soc. Jpn.* **77**, 014701 (2008).
- [34] Meysam Akhtar, George Anderson, Rong Zhao, Adel Alruqi, Joanna E. Mroczkowska, Gamini Sumanasekera, and Jacek B. Jasinski, "Recent advances in synthesis, properties, and applications of phosphorene," *npj 2D Mater. Appl.* **1**, 5 (2017).
- [35] See supplementary materials for more details.
- [36] X. Z. Yu, Y. Onose, N. Kanazawa, J. H. Park, J. H. Han, Y. Matsui, N. Nagaosa, and Y. Tokura, "Real-space observation of a two-dimensional skyrmion crystal," *Nature* **465**, 901 (2010).
- [37] Niklas Romming, Christian Hanneken, Matthias Menzel, Jessica E. Bickel, Boris Wolter, Kirsten von Bergmann, André Kubetzka, and Roland Wiesendanger, "Writing and Deleting Single Magnetic Skyrmions," *Science* **341**, 636 (2013).
- [38] M. C. Langner, S. Roy, S. K. Mishra, J. C. T. Lee, X. W. Shi, M. A. Hossain, Y.-D. Chuang, S. Seki, Y. Tokura, S. D. Kevan, and R. W. Schoenlein, "Coupled skyrmion sublattices in Cu_2OSeO_3 ," *Phys. Rev. Lett.* **112**, 167202 (2014).
- [39] M. Finazzi, M. Savoini, A. R. Khorsand, A. Tsukamoto, A. Itoh, L. Duò, A. Kirilyuk, Th. Rasing, and M. Ezawa, "Laser-induced magnetic nanostructures with tunable topological properties," *Phys. Rev. Lett.* **110**, 177205 (2013).
- [40] L.P. Jin, X. Chen, L. Zhou, J. Chen, H. He, G. Wang, D.P. Yu, B. Xi, F. Ye and J.W. Mei, "Topological paramagnetism in the ferromagnet embedded with spin-orbit-coupling nanosheets," to be submitted.
- [41] Andreas Bauer and Christian Pfleiderer, "Generic Aspects of Skyrmion Lattices in Chiral Magnets," in *Topological Structures in Ferromagnetic Materials: Domain Walls, Vortices and Skyrmions*, edited by Jan Seidel (Springer, Cham, 2016) (Springer, Cham, 2016).